

## Current status of the H<sub>2</sub> diffuse interstellar bands theory Assignments of the $\lambda\lambda$ 5780, 6284, 4428, 4882 large-equivalent-width diffuse interstellar bands

P. P. Sorokin,<sup>a†</sup> J. H. Glowonia<sup>a†</sup> and W. Ubachs<sup>b</sup>

<sup>a</sup> IBM Research Division, T. J. Watson Research Center, Yorktown Heights, NY  
10598-0218, USA

<sup>b</sup> Laser Centre, Vrije Universiteit, De Boelelaan 1081-1083, 1081 HV Amsterdam,  
Netherlands

---

Major changes recently incorporated into the structure of the non-linear H<sub>2</sub> DIBs model (P. P. Sorokin and J. H. Glowonia, *Astrophys J.*, 1996, **473**, 900) are outlined. To account for observed relative intensities of narrow DIBs assigned in the original model to H<sub>2</sub> inter-Rydberg transitions, it has become necessary to postulate a form of lightwave coherence existing in the H<sub>2</sub>-containing cloud of the model, with numerous coherent  $2n$  wave-mixing processes, each initiated by broadband stimulated Raman scattering (SRS), occurring on various H<sub>2</sub> transitions. By considering such wave-mixing processes, it becomes possible both to interpret archived VUV spectra of B-type supergiants and to easily assign large-equivalent-width DIBs (*e.g.*  $\lambda\lambda$ 5780, 6284, 4428, 4882) whose origins cannot be understood using the original ‘passive’ H<sub>2</sub> two-photon absorption model. The wave-mixing schemes discussed also enable one to understand why DIB intensities in given lines-of-sight correlate well with the amount of reddening observed in the same lines-of-sight.

---

### 1 Introduction

In a recently published article,<sup>1</sup> a new theory was presented attributing the diffuse optical interstellar bands (DIBs) (Fig. 1) to resonantly enhanced, simultaneous two-photon (VUV + VIS) absorption of light from a bright star by H<sub>2</sub> contained in a thin, tenuous cloud located relatively near the illuminating star. While it was shown in ref. 1 that the wavelengths of over 70 narrow DIBs could be matched to within the observational limits of error to calculated wavelengths of inter-Rydberg transitions in H<sub>2</sub>, the consensus of most astronomers (*e.g.* ref. 2) remained that these spectral matches were simply happenstance coincidences that did not provide any real credibility for the model. Within the past year, additional investigations were made with the aim of further testing the viability of the H<sub>2</sub> DIBs model. On the one hand, laboratory spectra were acquired [at Vrije Universiteit (VU)] of H<sub>2</sub> inter-Rydberg transitions that *a priori* would have been expected to correspond to DIBs according to the non-linear H<sub>2</sub> DIBs model of ref. 1. On the other hand, important changes in the structure of this model were proposed (at IBM) in an attempt to overcome some of the deficiencies that had become apparent in the original model. In making such changes, we have availed ourselves of a

† E-mail addresses: sorokin@watson.ibm.com; glowonia@us.ibm.com; wimu@nat.vu.nl

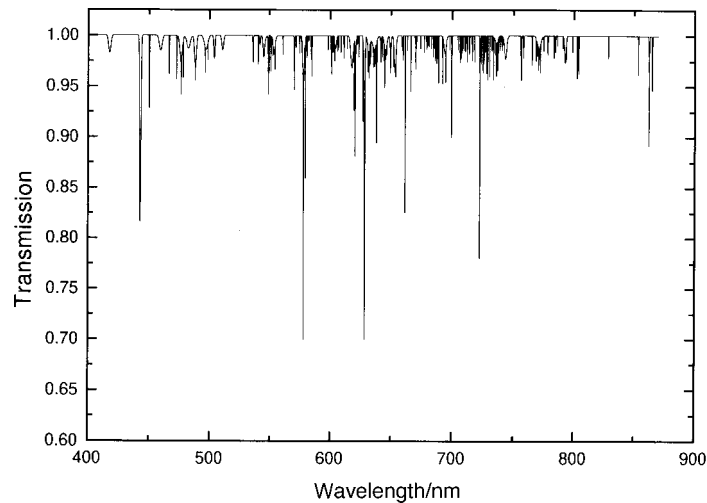


**Fig. 1** (DIB) spectrum from 3800–8680 Å for a line-of-sight of unit reddening. Spectrum synthesized from data contained in Table 3 of ref. 4.

variety of published spectral data that were not considered in ref. 1. These range from recent high-resolution spectral measurements of the lineshapes of the  $\lambda 5797$  and  $\lambda 6379$  DIBs to vacuum ultraviolet (VUV) spectra of mid-/late-B supergiants recorded in the 1970s. In this paper, we focus primarily on the changes that have been made in the past year in the original H<sub>2</sub> DIBs model and on the reasons why such changes were required.

## 2 The H<sub>2</sub> DIBs model<sup>1</sup>

Postulated in the model of ref. 1 was the existence of a thin H<sub>2</sub>-containing cloud located *ca.* 0.01–10 pc from a bright, early-type star and intersected by our line-of-sight to the star. It was argued that, in a collision-free medium, (a good approximation for the cold cloud with density *ca.*  $10^4 \text{ cm}^{-3}$  assumed in the model), elastic (*i.e.* resonance Rayleigh) scattering of near-resonant VUV starlight should completely dominate inelastic scattering (*i.e.* ‘absorption’ leading to real excitation of B- and C-state quantum levels) of the same light. (The theory of resonance fluorescence and light scattering is thoroughly discussed in ch. 8 of ref. 3, for example.) Consequently, near-resonant VUV light coming from the nearby hot star diffuses throughout the entire cloud, resulting in the steady-state flux column densities of this light along the line-of-sight to the star becoming greater than the values that would prevail in the total absence of the cloud. Conservation of energy dictates that ‘absorption’ of near-resonant VUV photons whose frequencies lie outside the *ca.*  $0.003 \text{ cm}^{-1}$  H<sub>2</sub> natural linewidth cannot occur *via* one-photon transitions. (For simplicity, Doppler broadening in the cloud of the model is assumed to be zero.) However, simultaneous two-photon absorption transitions to H<sub>2</sub> singlet-*gerade*-state quantum levels, involving both near-resonant VUV photons trapped by elastic scattering within the cloud and visible photons directly coming from the star, can exactly conserve energy and were assumed to occur in the model, producing the DIBs.

On the basis of the simple scheme described above, it became immediately possible to assign several dozen narrow DIBs to H<sub>2</sub> inter-Rydberg transitions. An example is the narrow DIB shown in Fig. 2. According to Table 3 of ref. 4, the frequency of this (+) (*i.e.* ‘certain’) DIB is  $12\,455.7 \pm 0.2 \text{ cm}^{-1}$  ( $8026.21 \pm 0.15 \text{ \AA}$ ), its linewidth is  $1.2 \pm 0.1 \text{ cm}^{-1}$ ,

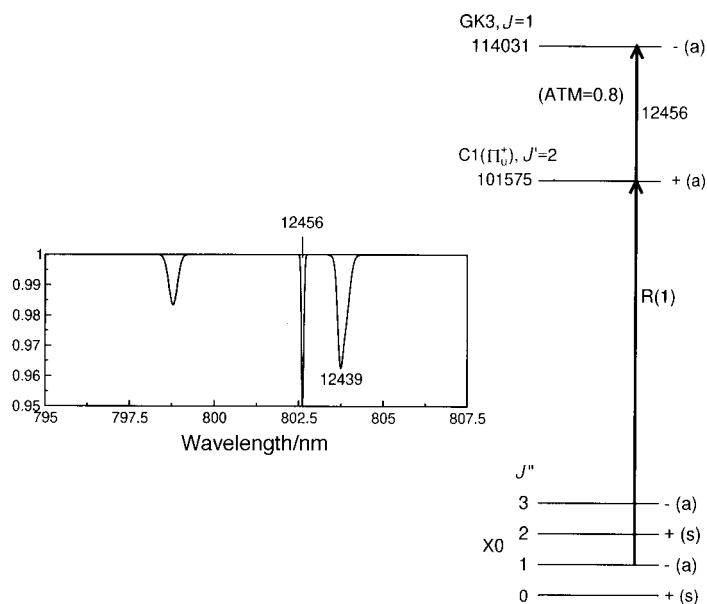


**Fig. 2** Diagram on right shows ref. 1 assignment of narrow DIB observed at *ca.*  $12456\text{ cm}^{-1}$ . An expanded portion of the spectrum in Fig. 1 containing this DIB is shown on the left. In all synthesized DIB spectra shown in this paper, DIBs with wavenumbers indicated were assigned in ref. 1.

and its equivalent width (in HD 183143) is  $52\text{ m}\text{\AA}$ . (Although the equivalent width is here relatively modest, the sharpness of this DIB allows it to be clearly seen in Fig. 1.) The exact frequency of the  $\text{H}_2$  inter-Rydberg transition to which this DIB is assigned in Fig. 2 can be calculated from the  $\text{H}_2$  quantum level energies tabulated in ref. 5–7. The value is  $12455.79\text{ cm}^{-1}$ , well within the narrow error limits given in ref. 4. In ref. 8, the frequency of this DIB is listed as  $12455.82 \pm 0.06\text{ cm}^{-1}$ .

Both the VUV and visible transitions shown in Fig. 2 have very large calculated radiative transition probabilities. For the C1–0R1 transition, which originates (as required in the model of ref. 1) from the very lowest quantum level of orthohydrogen ( $J'' = 1$  of X0), the value calculated<sup>9</sup> is  $0.14 + 9\text{ s}^{-1}$ . The strength of the visible transition shown is indicated by its large ‘adiabatic transition moment (ATM)’. (ATM values are calculated and tabulated for a variety of  $\text{H}_2$  transitions in ref. 10.) At first glance, the assignment in Fig. 2 seems quite compelling. However, a serious difficulty is present here that also occurs in most of the DIB assignments given in ref. 1. Briefly stated, no DIBs have thus far been observed that can be assigned to many other strong transitions originating from the same resonant intermediate-state quantum level,  $J' = 2(+)$  of C1. For example, no DIB is observed at  $12518.54\text{ cm}^{-1}$ , the calculated frequency of the  $\text{GK3} \leftrightarrow \text{C1 R}(2)$  transition. To us, this strongly implied that a mechanism based entirely upon ‘passive’ two-photon absorption by  $\text{H}_2$  molecules cannot adequately explain the origin of the DIBs. As will be explained in detail below, we currently assume that some form of coherent lightwave structure is present in the  $\text{H}_2$ -containing cloud of our model. In the case of Fig. 2, we would now suggest that broadband IR stimulated emission, spectrally centred on a transition connecting the  $\text{GK3}, J = 1$  quantum level with some lower-lying B- or C-state quantum level, must be occurring. We would now additionally postulate that this IR stimulated emission occurs as a step in an existing parametric oscillation cascade that ‘comes from above’, *i.e.* that starts at a higher-lying quantum level. Absorption of *ca.*  $12456\text{-cm}^{-1}$  photons would then occur *via* a process that should

probably be termed ‘four-photon inverse Raman absorption’, a four-photon analogue of the inverse Raman effect.<sup>11</sup> This mechanism should produce much stronger absorption of light at the DIB frequencies than passive two-photon absorption. Thus, in our current view, DIB selectivity can be the result of the operation of specific enhancement mechanisms.

Another DIB which was assigned in ref. 1 on the basis of a close frequency match is the narrow one ( $\Delta\nu \approx 2 \text{ cm}^{-1}$ ) appearing in Fig. 3 at *ca.*  $16135 \text{ cm}^{-1}$ . In ref. 4, the frequency of this much studied DIB is given as  $16134.4 \pm 0.9 \text{ cm}^{-1}$ . In ref. 8, the value listed is  $16135.12 \pm 0.05 \text{ cm}^{-1}$ . The value calculated for the H<sub>2</sub> transition to which the DIB is assigned in Fig. 3 is  $16135.06 \text{ cm}^{-1}$ . In terms of a frequency match with existing observations, the assignment is again seen to be a good one. However, in trying to account for the observed DIB intensity simply on the basis of a passive two-photon absorption model, one again encounters difficulty. The nature of this difficulty can be seen by comparing the two assignments shown in Fig. 2 and 3. For the B3–0P1 transition, which also originates from the lowest level of orthohydrogen, the calculated radiative transition probability<sup>12</sup> is  $0.10 + 9 \text{ s}^{-1}$ , about the same as for C1–0R1. However, the ATM for the visible transition in Fig. 3 is seen to be more than ten times smaller than that for the visible transition in Fig. 2. Nonetheless, the equivalent width of the DIB at  $16135 \text{ cm}^{-1}$  is *ca.*  $80 \text{ m}\text{\AA}$ , roughly 1.6 times greater than that of the DIB at  $12456 \text{ cm}^{-1}$ .

By discussing together the cases of the strong, but narrow,  $\lambda 5797$  and  $\lambda 6379$  DIBs, one can again illustrate both the strengths and the weaknesses of the H<sub>2</sub> DIBs model of ref. 1. The DIB at  $5797 \text{ \AA}$ , one of the most widely studied of the DIBs, was not actually assigned in ref. 1, since the air wavelength ( $5796.96 \text{ \AA}$ ) of the closest H<sub>2</sub> transition, *i.e.* the one originating from  $J' = 2$  of B0 and terminating on  $J = 3$  of EF12, appeared to lie outside the  $\lambda 5797$  DIB wavelength measurement error limits ( $5797.11 \pm 0.05 \text{ \AA}$ ) listed in ref. 4. However, subsequent very-high-resolution measurements of the  $\lambda 5797$  DIB presented in ref. 13 show this DIB to be *ca.* 2.4 wavenumbers wide and to be roughly peaked at  $5797.0 \text{ \AA}$ , a point at which the DIB profile displays a distinct sharp ‘notch’.

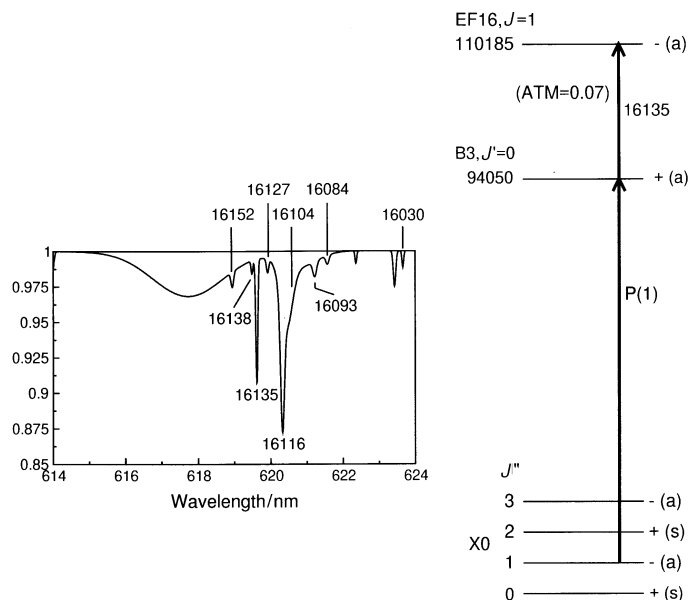


Fig. 3 Ref. 1 assignment and expanded spectrum for the DIB at *ca.*  $16135 \text{ cm}^{-1}$

This ‘notch’ is clearly seen in both lines-of-sight (*i.e.* towards  $\mu$  Sgr and towards  $\zeta$  Oph) for which the  $\lambda 5797$  DIB profile was recorded in ref. 13. The wavelength of this DIB is stated in ref. 8 to be  $5796.98 \pm 0.04$  Å. Thus, the more recent  $\lambda 5797$  DIB wavelength measurements lend strong support to the  $H_2$ -based assignment.

The  $\lambda 6379$  DIB was assigned in ref. 1 to the transition (EF10,  $J = 1$ )  $\leftarrow$  (B0,  $J' = 2$ ), that is, it was assigned to a transition having the same intermediate-state quantum level as in the above mentioned  $\lambda 5797$  DIB assignment. The calculated (air) wavelength of this transition is  $6379.23$  Å, within the error limits of ref. 4 ( $6379.27 \pm 0.08$  Å) and very nearly within those of Ref. 8 ( $6379.20 \pm 0.02$  Å).

Some observations were recently made that lend more interest to the fact that our assignments of the  $\lambda 5797$  and  $\lambda 6379$  DIBs feature the same intermediate-state quantum level. In ref. 14, the profile of the sharp  $\lambda 6379$  DIB was recorded at very high resolution in the line-of-sight to  $\zeta$  Oph. After telluric correction, this DIB showed a substructure described by the authors of ref. 14 as consisting of two equal peaks. However, the  $\lambda 6379$  DIB profile shown in this work can equally well be described as having a distinct sharp notch near its peak. In a still more recent high-resolution study of DIBs,<sup>15</sup> the presence of a clearcut notch at *ca.*  $6379.25$  Å on the  $\lambda 6379$  DIB was confirmed. An earlier study<sup>16</sup> was evidently the first to suggest that the  $\lambda 6379$  DIB possessed a two-peak structure.

The serious difficulty appearing to discredit the  $H_2$ -based assignments of both of these DIBs is, again, the lack of an explanation for the observed DIB intensities. Both  $\lambda 5797$  and  $\lambda 6379$  are among the strongest of the narrow DIBs. (In ref. 8, the equivalent widths in HD 183143 for  $\lambda 5797$  and  $\lambda 6379$  are listed as 238 and 123 mÅ, respectively.) Yet the strengths of the simultaneous two-photon absorption transitions involved in the DIB assignments are in both cases relatively weak. The B0–0R1 transition is the weakest of all B $n$ –0R1 transitions lying below the Lyman limit, being *ca.* 40 times weaker than C1–0R1, for example. In the simultaneous two-photon absorption model of ref. 1, the strength of the VUV transition influences both the intrinsic strength of the simultaneous two-photon absorption process and the density of near-resonant VUV photons trapped in the cloud by elastic scattering. In addition to the VUV transition being weak, the ATMs for the transitions (EF12,  $J = 3$ )  $\leftarrow$  (B0,  $J' = 2$ ) and (EF10,  $J = 1$ )  $\leftarrow$  (B0,  $J' = 2$ ) are also comparatively modest, being 0.04 and 0.15, respectively.

The processes illustrated in Fig. 4 represent a possible solution to the intensity anomaly problem discussed above. However, several unusual features requiring considerable explanation are involved. To begin with, as will be noted below, there exists fairly compelling spectral evidence that broad-band coherent VUV Stokes-wave emission occurs on the transition B0–0P3 in  $H_2$ -containing clouds near B-type giants and supergiants. This radiation would raise orthohydrogen molecules in  $J'' = 3$  of X0 to ‘virtual states’ lying near  $J' = 2$  of B0. From these virtual states, the molecules could be induced to follow pathways similar to the ones shown in Fig. 4. In Fig. 4, it is assumed that both quantum levels EF12,  $J = 3$  and EF10,  $J = 1$  are already involved in parametric oscillation cascades proceeding downward from higher levels. [For simplicity, in Fig. 4 we have specifically assumed a common IR cascade for the two levels, proceeding through  $J' = 2$  of B15. If the transition from EF12,  $J = 3$  to EF10,  $J = 1$  happened to occur as a degenerate two-photon emission process, the broad-band IR generated would be spectrally centred at  $787$  cm<sup>-1</sup>, the frequency of one of the ‘unidentified IR emission bands (UIBs)’ discovered in ref. 17.] With strong broad-band light waves present that are spectrally centred on the topmost two IR transitions in Fig. 4, and with strong broad-band VUV light around B0–0P3 also present, one expects that light around  $5797$  Å will be absorbed through the same ‘four-photon inverse Raman absorption’ process already briefly mentioned above. A similar process would produce the  $\lambda 6379$  DIB. From the unspecified singlet-*ungerade*-state quantum level shown in Fig. 4, the downward parametric oscillation cascade would continue in some manner, eventually returning the molecules to  $J'' = 3$  of X0.

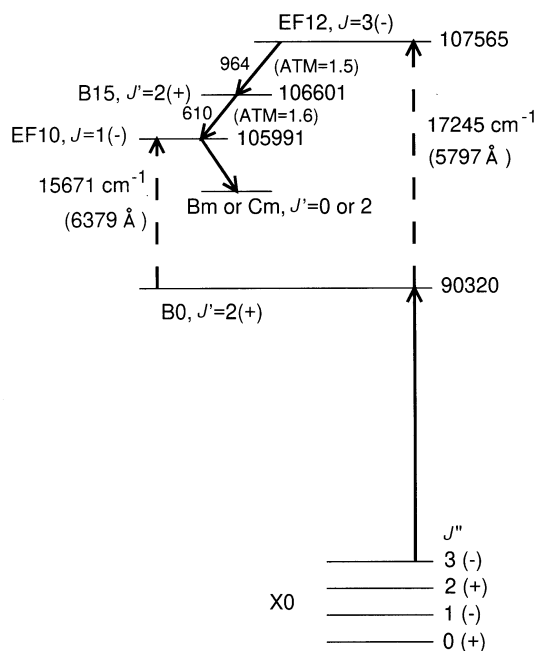


**Fig. 4** Wavemixing processes incorporating inverse Raman absorption steps proposed in text to explain selective enhancement of  $\lambda 5797$  and  $\lambda 6379$  DIB intensities

On the basis of the scheme shown in Fig. 4, one can thus account for the relatively strong  $\lambda 5797$  and  $\lambda 6379$  DIB intensities that are observed, for the fact that the intensities of these DIBs are strongly correlated with reddening in the line-of-sight (explanation to be given below), and for the fact that there, here again, must be some mechanism that restricts the number of DIBs. No DIBs are observed that correspond to the frequencies of the transitions (EF12,  $J = 1$ )  $\leftarrow$  (B0,  $J' = 2$ ) or (EF10,  $J = 3$ )  $\leftarrow$  (B0,  $J' = 2$ ), for example. In the present instance, it is again seen that selectivity results from the presence of enhancement mechanisms.

In global terms, the model outlined in ref. 1 is far more inadequate than has thus far been represented. We have described the severe intensity anomalies present in some of the assignments of narrow DIBs. However, on the basis of the model of ref. 1, most of the prominent, large-equivalent-width DIBs appearing in Fig. 1 cannot be assigned at all. Several of the DIBs have very broad linewidths, of the order of 50 wavenumbers or more. In ref. 1, only speculative arguments were offered to explain the origin of DIBs with such large linewidths. It was suggested that the cause of this width might be found in the rapid rates of predissociation and/or autoionization of singlet-*gerade*-state quantum levels lying higher in energy than  $118\,375.6\text{ cm}^{-1}$ , the threshold for dissociation into H(1s) + H(2s, 2p). The various double-resonance measurements described in the next section have generally dispelled both this notion and several others that were contained in ref. 1.

### 3 H<sub>2</sub> double resonance measurements

In ref. 18, double resonance (VUV + VIS) ionization spectra of H<sub>2</sub> were reported which showed a number of coincidences (*i.e.* frequency and linewidth matches) with modest-equivalent-width DIBs (Fig. 5). The matching DIBs have only been reported in ref. 4, however. Both C5 and C6 quantum levels were excited from X0 with the VUV laser

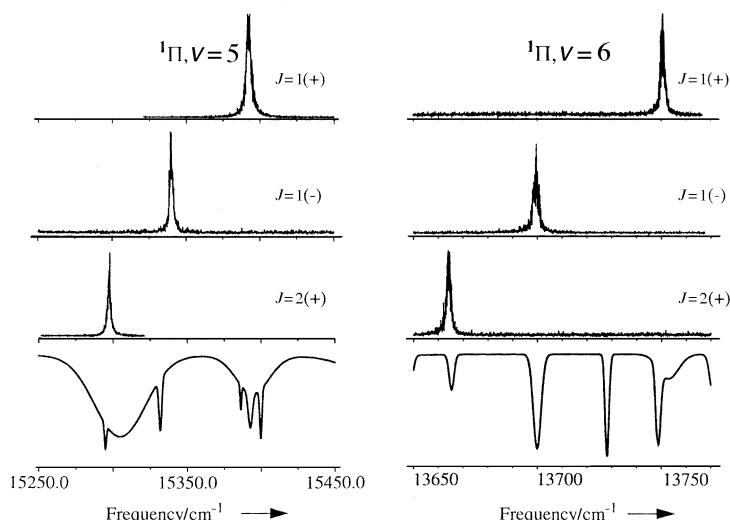


**Fig. 5** Double-resonance ionization spectra probing singlet-*gerade*-state quantum levels lying above the ionization threshold. The VUV laser was tuned to C5 intermediate states (left) and C6 intermediate states (right). The bottom spectra show expanded portions of the DIB spectrum of Fig. 1 corresponding to the same wavelength ranges.

separately tuned to each of the R(0), R(1), and Q(1) transitions. With the VUV laser frequency set to coincide with a given absorption line, a tunable visible laser was then scanned in frequency, and a photoionization spectrum was recorded. Singlet-*gerade*-state quantum levels lying in a region just above the H<sub>2</sub> autoionization threshold (124 418.4 cm<sup>-1</sup>) were probed.

Somewhat remarkably, it was found that in a spectral range spanning *ca.* 1000 cm<sup>-1</sup> in an energy region where the H<sub>2</sub> density-of-states might *a priori* be expected to be high, only the strong resonances shown in Fig. 5 were seen. Four of these transitions terminate on a singlet-*gerade*-state quantum level of orthohydrogen (configuration unknown) located at 124 752.5 cm<sup>-1</sup>. The other two both terminate on a quantum level of parahydrogen (presumably, a different rotational level belonging to the same configuration as above) at 124 701.9 cm<sup>-1</sup>. The linewidths of all six resonances, and of the five DIBs which seemed to match, were all between 2 and 3 wavenumbers. These widths undoubtedly reflect the rates of autoionization of these two quantum levels.

One can attempt to discuss the resonances appearing in Fig. 5 in terms of the basic model of ref. 1. To begin with, all three C5–0 transitions [*i.e.* R(0), R(1), and Q(1)] lie below the Lyman limit (91.2 nm). These transitions should, therefore, be potentially excitable in the H<sub>2</sub>-containing cloud assumed in the model of ref. 1. The equivalent widths (in HD 183143) of the two DIBs which seem to correspond to the top and bottom C5 resonances in Fig. 5 are stated in ref. 4 to be 24 and 12 mÅ, respectively. Since the ratio of these equivalent widths is about the same as the ratio (1.82) of the C5–0Q1 and C5–0R1 transition probabilities, it would seem, at first glance, that this particular pair of DIB assignments can be more-or-less understood on the basis of the original ‘passive’ two-photon absorption model of ref. 1. The middle C5 resonance is much too far off resonance (*ca.* 9 cm<sup>-1</sup> difference) from the closest DIB appearing in Fig. 5 to be even remotely considered a frequency match. This DIB, which has a frequency of 15 331.5 cm<sup>-1</sup> and an equivalent width of 30 mÅ was reasonably assigned in ref. 1 as the R(2) transition of EF13 ↔ B2. However, one is now required to explain the absence of an observed DIB corresponding to the middle C5 resonance. At this point,

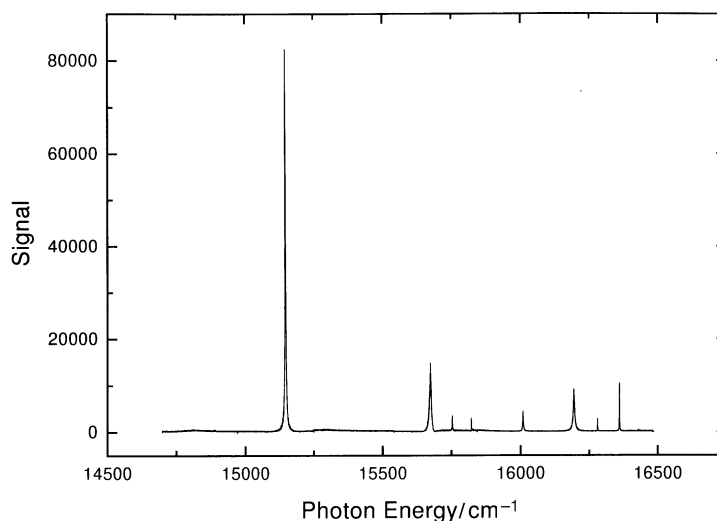


**Fig. 6** Double-resonance ionization spectrum probing singlet-*gerade*-state quantum levels lying below the ionization threshold. The VUV laser was here tuned to the C2-0R1 line. (Spectral data from ref. 21.)

we can only postulate that broad-band stimulated Raman scattering (SRS) involving C5,  $J' = 1(-)$  as resonant intermediate state must be occurring in the H<sub>2</sub>-containing clouds in which the DIBs originate. According to ref. 19, when the intermediate quantum level in a resonant two-photon absorption process is radiatively coupled by a light wave to a fourth quantum level, the probability of simultaneous two-photon absorption occurring from the ground level to the two-photon level may be reduced by many orders of magnitude. This effect is a two-photon analogue of 'electromagnetically induced transparency (EIT)', a topic of current theoretical interest. (See, *e.g.* ref. 20.) It is thus seen that, with the assumption of a coherent lightwave structure present in the H<sub>2</sub>-containing cloud, there is the potential for both DIB-enhancing and DIB-attenuating mechanisms to exist.

It is more awkward to try to explain the three apparent coincidences of DIBs with transitions involving C6 seen in Fig. 5. [The narrow DIB at *ca.* 13 718 cm<sup>-1</sup> was assigned in ref. 1 to the strong (ATM = 0.95) transition  $\text{H}\bar{\text{H}} \leftrightarrow \text{C2}, \text{Q}(2)$ .] All three C6-0 transitions lie at shorter wavelengths than the VUV cut-off imposed by the Lyman limit. We speculate that virtual states near the C6 levels are excited by VUV light existing in the cloud at certain wavelengths longer than 91.2 nm (*vide infra*). This VUV light promotes transitions of molecules existing in vibrationally excited levels of the X state. The latter are populated in primary VUV SRS processes of the type to be discussed in detail below.

From the strong resonances seen in Fig. 5, one would guess that the potential curve for the unknown singlet *gerade* state is similar in shape to the C-state potential curve, only vertically shifted from the latter to higher energies. This, in turn, would imply that strong transitions between the same two states could, in principle, occur from lower C-state vibronic levels to correspondingly lower vibronic levels of the singlet *gerade* state. However, the energies of these lower singlet-*gerade*-state vibronic levels would lie below the threshold for H<sub>2</sub> autoionization. One would, therefore, not expect signals to be generated at resonances using the experimental arrangement employed in ref. 18. However, by modifying the technique used in ref. 18 to include an extra pulse for ionizing H(2s,2p) atoms produced in H(1s) + H(2s,2p) dissociation channels, the group at VU has now shown<sup>21</sup> that transitions from C-state vibronic levels to singlet-*gerade*-state

vibronic levels lying between the energy thresholds for dissociation into  $H(1s) + H(2s,2p)$  and autoionization into  $H_2^+ + e^-$  can easily be observed. (In unpublished earlier work,<sup>22</sup> several  $H_2$  resonances in this same range were observed with use of a similar technique.)

Fig. 6 shows an example of an ionization spectrum obtained in this manner.<sup>21</sup> Although striking resonances are seen here, it turns out that there are no correspondences with DIBs. One can again reasonably propose that SRS involving  $C2, J' = 2(+)$  as resonant intermediate state might be occurring, and that consequently (again, by the main result derived in ref. 19) the intensity of two-photon absorption from  $J'' = 1$  of X0 to any of the singlet-*gerade*-state quantum levels located by the resonances in Fig. 6 will be greatly diminished. However, considering all the double-resonance experiments which have here been described, one senses the futility of attempting to explain the origins of large-equivalent-width DIBs (especially the very broad ones) on the basis of rapidly dissociating and/or autoionizing singlet-*gerade*-state quantum levels existing in heretofore unexplored energy ranges. In the remainder of this paper we outline a promising new approach we have recently been following in seeking to provide an  $H_2$ -based answer to this question.

#### 4 Evidence for nonlinear generation of VUV light in $H_2$ -containing clouds near B-type supergiants

If mechanisms involving coherent light generation are required to explain the observed DIB relative intensities, it becomes a reasonable investigative step to examine archived VUV spectra of bright stars for some evidence of VUV light generation actually occurring in these stars. In a manuscript recently submitted for publication,<sup>23</sup> we indicate that it is indeed possible to interpret some of the spectral data obtained by various VUV space probes (*e.g.* Copernicus and ORFEUS-1<sup>24</sup>) to show that, in clouds surrounding some B-type stars, both SRS and a related process known as four-wave parametric oscillation (FWPO) ubiquitously occur on  $H_2$  transitions in a manner closely resembling some of the scenarios that were briefly considered in ref. 1, and that these processes can actually represent ‘main events’ determining the spectral character of these objects in the VUV.

We began outlining this evidence in ref. 23 by showing that, for some stars located high above the galactic plane (‘halo stars’), whose lines-of-sight would thus be less likely to be intersected by interstellar  $H_2$  clouds that are far removed from the stars themselves, the observed intensity ratios of individual  $Bn \leftarrow X0$  R(0), R(1), and P(1) transitions cannot be comprehended on the basis of linear spectroscopy. This can be seen, for example, in the ORFEUS-1 spectrum of the B1 Ib halo star ( $d = 1.7$  kpc) HD 214080 (Fig. 7 and 8). Comparing these two figures, one observes that the B0–0 absorption components are clearly stronger than those of B4–0. Yet the calculated radiative transition probabilities<sup>12</sup> of the latter are *ca.* 16 times those of the former. From this clear anomaly, which is also apparent in the VUV spectra of several other B-type stars that were probed by ORFEUS-1, we infer that there exist ubiquitously in our galaxy spectrally accessible clouds of  $H_2$  for which paradigms based upon the Copernicus high-resolution VUV spectrum of  $\zeta$  Oph shown in ref. 25 are not relevant. The tentative explanation we offer for the strong enhancement of individual R(0), R(1), and P(1)  $Bn-0$  absorption components that is observed for select low  $n$  in many B-type stars involves SRS processes occurring on some of these transitions. This will be discussed further in what follows.

In ref. 26, Copernicus low-resolution (0.2 Å) observations of 16 O-type stars and 10 B-type stars (mostly supergiants) covering the range 1000–1200 Å are presented in the form of a classical spectral atlas. In ref. 23, we focussed on what appeared to be a few

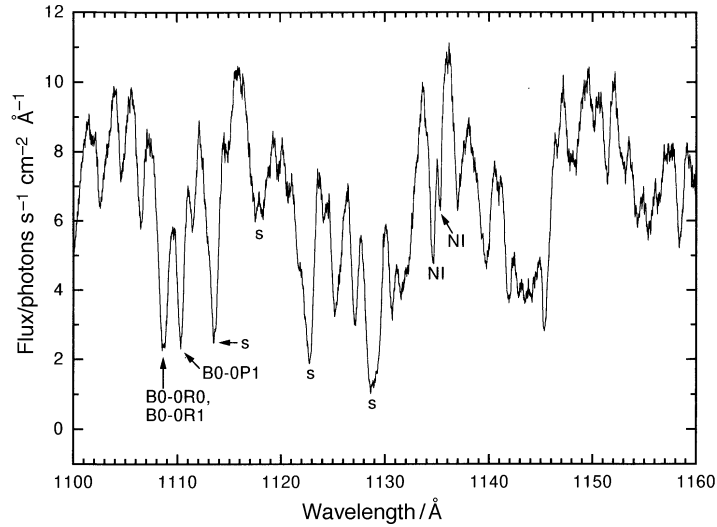


**Fig. 7** Expanded view of a section of the ORFEUS-1 HD 214080 spectrum. Absorptions marked 's' are of known stellar origin. Two interstellar N I absorption lines are indicated.

dozen emission lines rising well above the background continuum in the mid-/late-B supergiant spectra shown in ref. 26 (Fig. 9). There seemed to exist no specific identifications or assignments of these apparent emission features in the scientific literature. However, we have recently learned that it has long been the general opinion of the astrophysical community (see, for example, ref. 27) that (1) no emission lines are present in spectra such as those shown in Fig. 9; (2) the background VUV continuum level should always be placed at the level of the very highest peaks that are observed; and (3) the resulting large fraction of continuum light which is thus inferred to be missing is

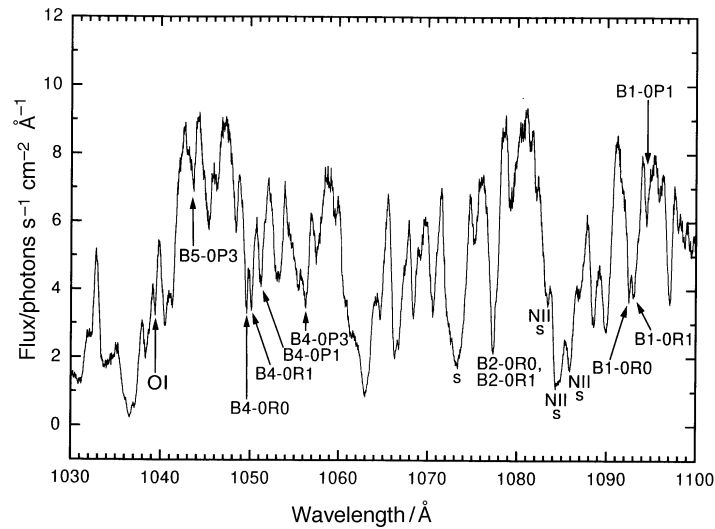


**Fig. 8** Expanded view of a section of the ORFEUS-1 HD 214080 spectrum adjacent to that shown in Fig. 7. Absorptions marked 's' are of known stellar origin. An interstellar O I line is marked.

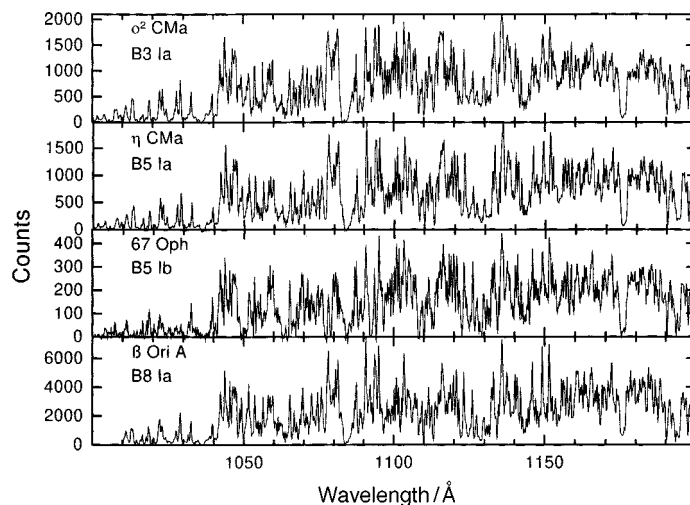


**Fig. 9** Copernicus low-resolution VUV spectra of four mid-/late-B supergiants as shown in Fig. 6 of ref. 26

absorbed by over 1000 blended stellar photospheric absorption lines, mostly due to ions of transition metals. Despite this interpretation, we here proceed to describe some of the interesting consequences that follow if one assumes that emission peaks are indeed present in the spectra of Fig. 9.

Fig. 10 shows a wavelength-expanded portion of Fig. 9 containing one of the most intense ‘emission’ peaks appearing in the latter. This peak appears in each spectrum of Fig. 10 at a wavelength that is very close to 1135.9 Å. Making the assumption that this peak must be nearly centred on the wavelength of an allowed transition of H<sub>2</sub>, and that low rotational quantum numbers must be involved, one concludes from inspection of Table 61 of ref. 28 that the most likely transition is B8–3R0 at 1135.90 Å. In ref. 23, it was assumed that this emission peak was generated as a Stokes wave in a resonantly enhanced stimulated Raman scattering process. This SRS process would result from broadband optical pumping of ground-state parahydrogen molecules by VUV photons in the H<sub>2</sub>-containing cloud that are nearly resonant with B8–0R0. As has already been explained, it is generally assumed in all of our DIB models that enhanced densities of nearly-resonant VUV photons exist throughout the cloud as a result of elastic (*i.e.* Rayleigh) scattering.

Ref. 27 features a high-resolution (0.05 Å, *i.e.* 5 cm<sup>-1</sup> at *ca.* 1000 Å) Copernicus scan of β Ori A from 999 to 1561 Å. In this scan, the width of the 1135.9 Å peak appears to be 50–60 cm<sup>-1</sup>. Since Doppler broadening of VUV fluorescent lines emitted by H<sub>2</sub> molecules residing in the thin cloud of our model should be at least 10 to 100 times smaller than this, one can conclude that if the 1135.9 Å emission band is indeed due to H<sub>2</sub>, it is generated not through normal fluorescence, but through a mechanism such as broad-band SRS or FWPO.

Another prominent emission peak in Fig. 10 is seen to occur ubiquitously at *ca.* 1116 Å. This emission band also appears strongly in all the ORFEUS-1 spectra of B-type giants and supergiants we have examined. (See, *e.g.* Fig. 11.) From Table 58 of ref. 28, we assign this peak to B0–0P3 at 1115.9 Å. We speculated in Section 2 that generation of coherent light on this transition should play an important role in determining the absorption strengths of the λ5797 and λ6379 DIBs.

In Fig. 11, the ORFEUS-1 spectrum of the (B1 Ib) star HD 214080 is compared with the Copernicus spectrum of β Ori A in the same wavelength range shown in Fig. 10.

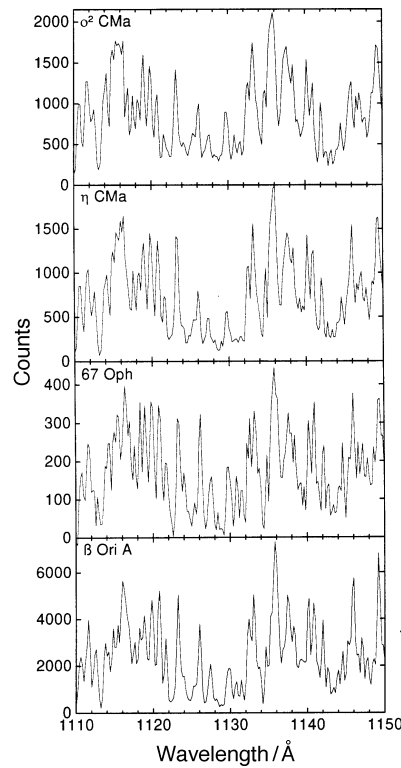
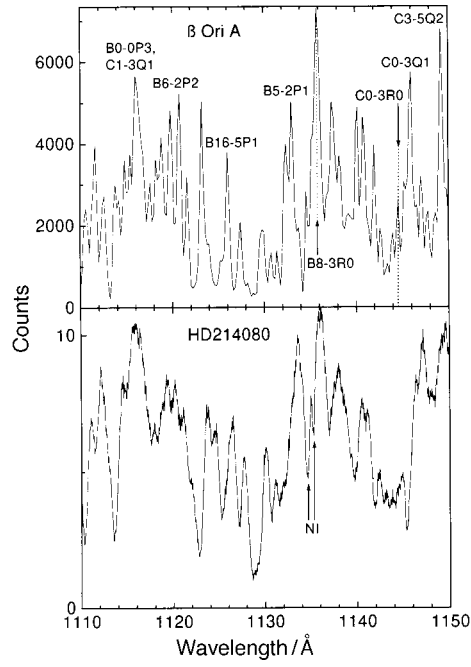


Fig. 10 Expanded view of a section of the Copernicus spectra shown in Fig. 9

While the (emission peak height/ background continuum level) ratio is clearly less in the case of the much hotter ORFEUS-1 star, the major peaks are seen to occur at approximately the same wavelengths as in Fig. 10. One becomes more easily convinced of the existence of emission peaks viewing the  $\beta$  Ori A spectrum, however. All other assignments of peaks shown in Fig. 11 result from analysing the higher-resolution  $\beta$  Ori A spectrum shown in ref. 27 with the same method used above in assigning the 1135.9 Å peak.

In Fig. 12, wavelength-expanded portions of two of the spectra appearing in Fig. 9 are shown in another spectral range. One sees again that the major peaks occur at exactly the same wavelengths in these two different temperature stars. Two of the emission peaks in this figure (at *ca.* 1043.9 Å and *ca.* 1065.2 Å) are assigned as Stokes waves in SRS processes having the same initial and final states as the SRS process proposed above as the generating mechanism for the 1135.9 Å emission peak. However, in order for SRS to occur on a continuous basis, some effective mechanism must exist to depopulate the terminal state and repopulate the ground state. A possible mechanism in this case would be that shown in Fig. 13. The essential idea here is that additional SRS and/or inverse Raman and/or parametric oscillation steps are required in order to deplete continuously the population of molecules pumped to  $J'' = 0$  of X3 and to provide a return path for this population back to  $J'' = 0$  of X0. With the incorporation of such additional steps, the overall process can no longer be described as being simple broad-band SRS. It must, instead, be viewed as a type of hybrid wave-mixing process, in which SRS pumping, absorption resulting from inverse Raman scattering, or parametric oscillation can each occur at more than one step. In ref. 23 we employed the term 'SRS-FWPO' to describe such hybrid processes. The hybrid process may involve four



**Fig. 11** Expanded Copernicus  $\beta$  Ori A spectrum of Fig. 10 compared with the ORFEUS-1 spectrum of HD 214080 over the same spectral range. Two interstellar N I lines are indicated in the latter spectrum.

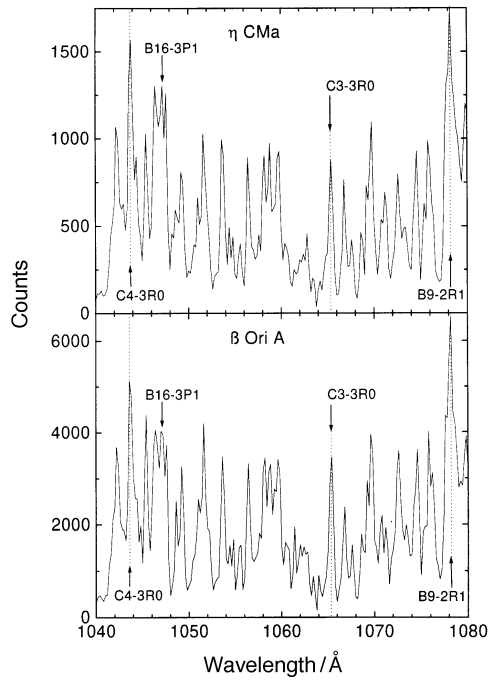


**Fig. 12** Expanded view of a section of the Copernicus spectra of two of the stars shown in Fig. 9. A few emission bands discussed in the text are shown.

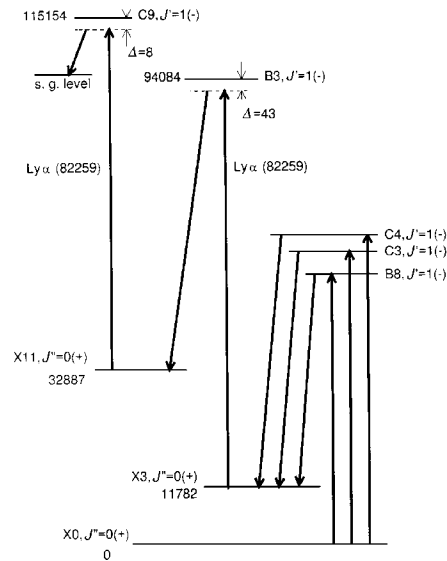


**Fig. 13** An SRS-FWPO wavemixing scheme that can account for continuous SRS Stokes-wave emission on B8–3R0, C4–3R0, and C3–3R0.

waves, six waves, eight waves, or more. In Fig. 13, it is assumed that a downward parametric oscillation cascade continues from an unspecified singlet-*gerade*-state quantum level (the ‘s.g. level’ in Fig. 13), eventually terminating on  $J'' = 0$  of X0.

All waves participating in SRS–FWPO processes of the type shown in Fig. 13 must be colinear, a basic requirement that follows from momentum conservation. In the thin H<sub>2</sub>-containing cloud of our model, this implies that all waves participating in SRS–FWPO processes must propagate in the plane of the cloud. This restriction will form the basis for the explanation proposed in the next section for the universally observed dependence of DIB intensity upon reddening in the line-of-sight.

In Fig. 13, it is assumed that intense pumping radiation in the vicinity of Ly- $\alpha$  exists in the cloud. A relatively high density of H atoms is assumed to exist in the cloud, and elastic scattering of VUV radiation near Ly- $\alpha$ , Ly- $\beta$ , ... *etc.* by these atoms will result in there being present in the cloud greatly concentrated densities of photons that are nearly resonant with these transitions. Note that, owing to the isotropic nature of the elastic scattering process, there will always be Ly- $\alpha$ , Ly- $\beta$ , Ly- $\gamma$ , ... *etc.* photons propagating in the plane of the cloud. These photons can therefore participate in SRS–FWPO processes.

Let us restate the general hypothesis that has evolved from the discussion of Fig. 13 just presented. If there happens to exist a near-coincidence in frequency between either Ly- $\alpha$ , Ly- $\beta$ , or a higher-lying H-atom resonance line and a strong transition to some higher-lying singlet-*ungerade*-state quantum level from the particular X-state quantum level that is populated by a given Stokes-wave emission, an effective SRS–FWPO pathway capable of depleting the X-state quantum level may exist, allowing the VUV SRS to occur. On the basis of this general hypothesis, it appears to be possible to justify most of the H<sub>2</sub>-based assignments we have thus far made. Consider, for example, the emission peak appearing at *ca.* 1126 Å in Fig. 11, which we have assigned as a broadband SRS Stokes-wave emission occurring on B16–5P1. (The exact wavelength of the B16–5P1 transition is 1126.085 Å.) The primary SRS process would here be pumped by VUV photons nearly resonant with the strong transition B16–0P1. According to our model, the densities of such photons everywhere in the cloud should be greatly enhanced

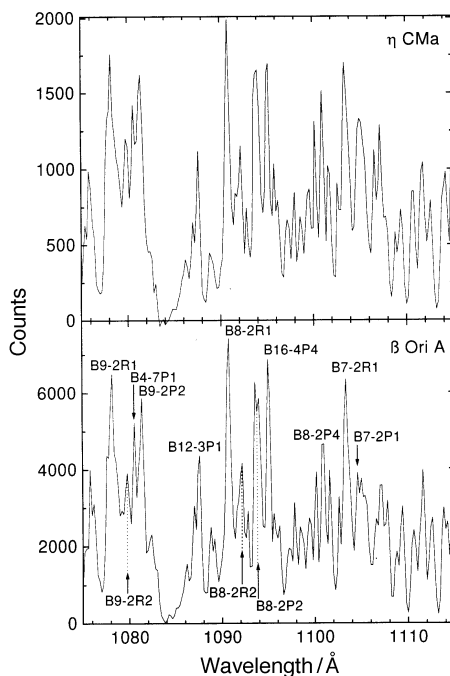


**Fig. 14** Expanded view of another section of the Copernicus spectra of two of the stars shown in Fig. 9. Several emission bands assigned in the text are shown.

through elastic scattering. There are several B16-*n*P1 transitions considerably stronger than B16-5P1, which should have correspondingly higher Stokes-wave gains, but to which none of the emission peaks in the spectra of late-/mid-B supergiants actually seem to correspond. A plausible explanation can be offered for this unusual selectivity in terms of the general SRS-FWPO scheme here being proposed. If one adds the energy of a Ly- $\alpha$  photon ( $82\,259\text{ cm}^{-1}$ ) to the energy<sup>29</sup> of the X5,  $J'' = 1$  quantum level ( $18\,582\text{ cm}^{-1}$ ), the result is  $100\,841\text{ cm}^{-1}$ . The energy of the B9,  $J' = 0$  quantum level is  $100\,843\text{ cm}^{-1}$ , just two wavenumbers away. The B9,  $J' = 0$  level could thus effectively serve as the resonant intermediate state in a secondary SRS process originating from X5,  $J'' = 1$ . The secondary Stokes wave could be generated either in the IR, for example, on the (ATM = 0.13) transition (B9,  $J' = 0$ )  $\rightarrow$  (EF1,  $J = 1$ ) at *ca.*  $1467\text{ cm}^{-1}$ , or in the VUV, on a transition that drops the molecules back to some vibronic level of the X state. Since Stokes-wave gain generally varies as  $\rho^2\nu$  where  $\rho$  is the transition dipole moment and  $\nu$  is the frequency of the Stokes-wave transition, VUV generation would *a priori* be heavily favoured, except that, once more, some mechanism must exist that is capable of depopulating the terminal state of the secondary SRS process. Relaxation of the secondary SRS terminal state is not a problem in the case of IR Stokes-wave generation, since EF vibronic levels can decay on a nanosecond timescale to lower-lying B- and C-state quantum levels. We are unable to specify with any accuracy an exact pathway for the SRS-FWPO process in the present instance. However, a reasonable speculation would be that the secondary Stokes-wave emission occurs on B9-4P1 at  $1169.6\text{ \AA}$ . There is an emission peak seen at this wavelength in the spectra of the mid-/late-B supergiants. Moreover, when one adds the energy of a Ly- $\alpha$  photon to the energy of the X4,  $J = 1$  quantum level ( $15\,346\text{ cm}^{-1}$ ), one gets  $97\,605\text{ cm}^{-1}$ , just 14 wavenumbers away from B6,  $J' = 0$  at  $97\,591\text{ cm}^{-1}$ . The Stokes wave in a tertiary SRS process employing B6,  $J' = 0$  as resonant intermediate state would necessarily have to occur in the VUV, since there

are no EF vibronic levels below B6,  $J' = 0$ . We speculate that the Stokes-wave emission might here occur on B6–11P1 at 1546.7 Å. This has a large calculated radiative transition probability, and an emission peak is seen at this wavelength in ref. 27. Moreover, from X11,  $J = 1$ , a Ly- $\alpha$  photon reaches an energy of 115 197 cm<sup>-1</sup>, just 25 wavenumbers away from C9,  $J' = 2(+)$  at 115 222 cm<sup>-1</sup>. This quaternary SRS process involving orthohydrogen molecules thus perhaps proceeds in a manner generally similar to the tertiary SRS process involving parahydrogen molecules shown in Fig. 13.

In Fig. 14, wavelength-expanded portions of two of the spectra shown in Fig. 9 are presented in yet another spectral range. On the basis of the high-resolution  $\beta$  Ori A spectrum contained in ref. 27, we have again assigned many of the most prominent peaks shown here. Four of the transitions assigned as Stokes-wave emissions in this figure (B9–2R1, B8–2R1, B7–2R1, and B7–2P1) have the same SRS terminal state,  $J'' = 1$  of X2. Molecules brought to this terminal state by the primary SRS processes can be redirected back to the SRS ground state through the SRS–FWPO process shown in Fig. 15. In this case, pumping light for the secondary SRS process is provided by the enhanced densities of photons in the cloud that are nearly resonant with Ly- $\beta$ . An emission band whose frequency corresponds to the last leg (B10–0P1) of the SRS–FWPO process illustrated in Fig. 15 can be seen in ORFEUS-1 spectra of B-type stars (Fig. 16). In Fig. 16, a notch can be discerned on the emission band at the exact frequency of the B10–0P1 line centre. Parametric oscillation normally develops in such a manner that gain is optimized and loss is minimized. Therefore, to avoid loss associated with real absorption occurring within the natural linewidth, or elastic scattering occurring at larger frequency offsets, a notch in the VUV emission band forms at the exact position of the B10–0P1 line centre.

In ref. 23, another SRS–FWPO pathway capable of depleting the population in X2,  $J'' = 1$  was discussed. In this alternative scheme, the secondary SRS Stokes-wave emission occurs in the VUV. The secondary SRS intermediate state is the same,  $J' = 1(+)$  of C3.

The SRS process which produces the prominent Stokes-wave emission peak assigned as B16–4P4 in Fig. 14 is somewhat unusual. In this case, the molecules that are excited to undergo SRS are parahydrogen molecules occupying the X0,  $J'' = 2$  quantum level.

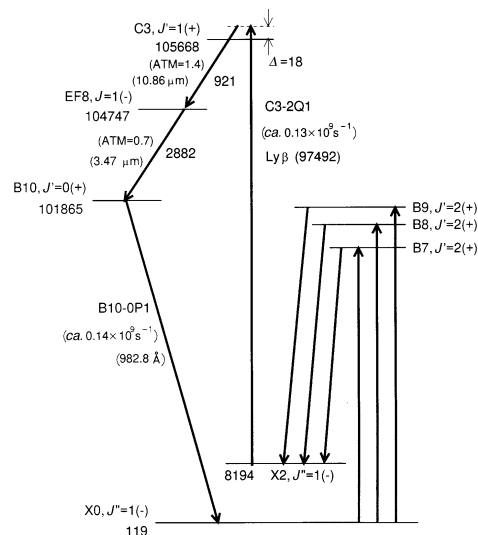


**Fig. 15** A possible SRS–FWPO process discussed in the text capable of generating emission on the transitions B9–2R1, B8–2R1, B7–2R1 and B10–0P1

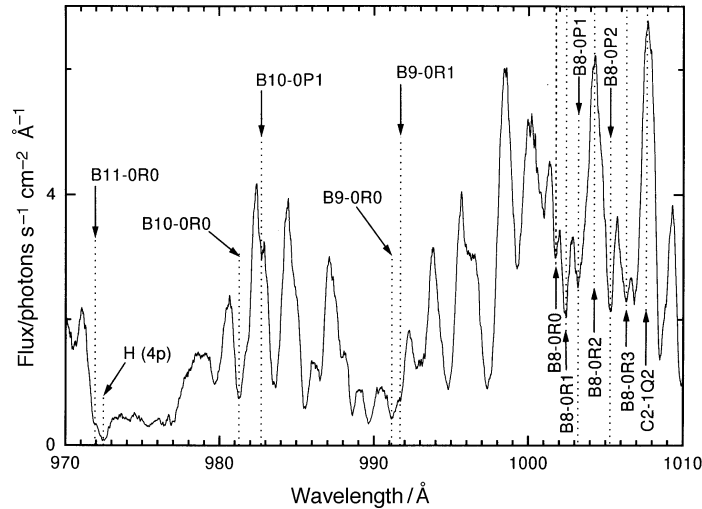


**Fig. 16** Expanded view of a section of the ORFEUS-1 spectrum of HD 214080. The marked emission peaks and absorption regions are assigned in the text to the H<sub>2</sub> transitions indicated.

The pumping transition is B16-0R2 at 933.2 Å. Some evidence of non-linear absorption occurring around this wavelength can be seen in the ORFEUS-1 spectra of B-type stars (Fig. 17). However, adding the photon energies of either Ly- $\alpha$ , Ly- $\beta$ , or Ly- $\gamma$  to the energy of the X4,  $J'' = 4$  quantum level (16 191 cm<sup>-1</sup>) results in an energy that is far removed from that of any singlet-*ungerade*-state quantum level optically connected to  $J'' = 4$  of X4. To achieve resonance, one has to add the energy of a Ly- $\delta$  photon, 105 292 cm<sup>-1</sup>. The frequency of the strong D4-4Q4 transition is 105 289 cm<sup>-1</sup>.<sup>30</sup>

It is also possible to explain some of the absorption and emission features seen in the Copernicus and ORFEUS-1 spectra using FWPO processes of the simpler type that were considered in ref. 1. For example, Fig. 18 shows a simple FWPO process characterized by high radiative transition probabilities which should lead to emission around

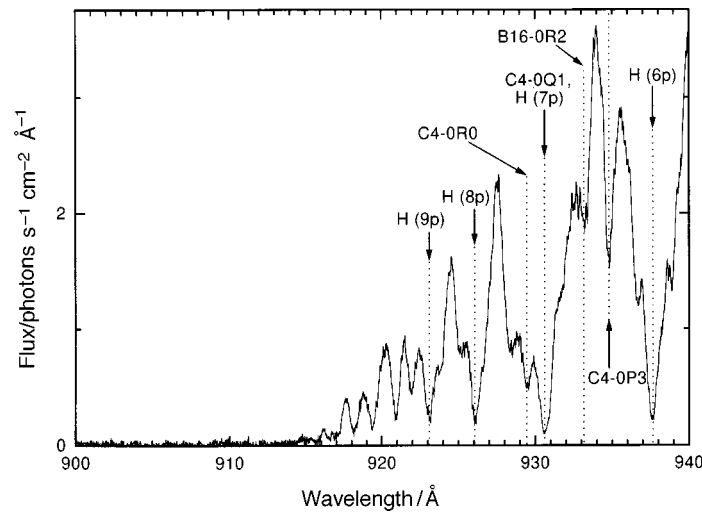


**Fig. 17** Expanded view of a section of the ORFEUS-1 spectrum of HD 214080 extending to the Lyman limit (91.2 nm). The H<sub>2</sub> transitions marked are discussed in the text.

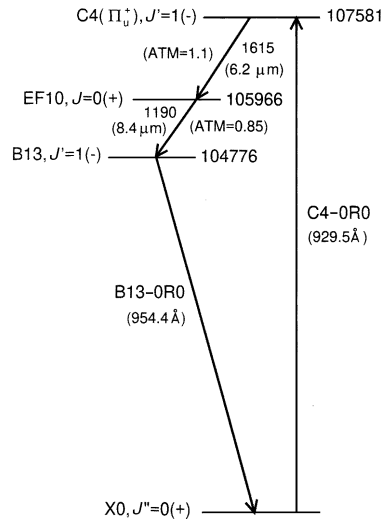


**Fig. 18** A possible simple FWPO process that could generate VUV emission on B13-0R0

954.4 Å and absorption around 929.5 Å. In Fig. 19, a prominent emission band is seen corresponding to the B13-0R0 wavelength, but the observed absence of any hint of a notch is somewhat puzzling. In Fig. 17, there appears to be a fairly well defined absorption region corresponding to C4-0R0 at 929.5 Å. There may also exist some evidence of C4-0Q1 absorption at 930.6 Å in Fig. 17, but this is somewhat hard to discern, in view of the H(7p) absorption occurring at 930.75 Å. Significantly, there appears to be no hint of absorption corresponding to C4-0R1 at 929.7 Å, although the calculated radiative transition probabilities of C4-0R0 and C4-0R1 are roughly similar. We will refer again to this observation in discussing our assignment of the  $\lambda$ 4428 and  $\lambda$ 4882 DIBs in the next section.

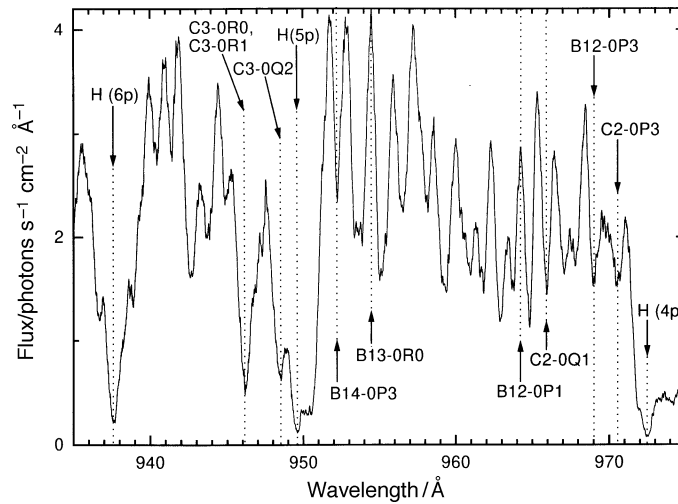


**Fig. 19** Expanded view of a section of the ORFEUS-1 spectrum of HD 214080. An emission peak and several regions of absorption are assigned in the text to the H<sub>2</sub> transitions indicated.

### 5 Assignments of the $\lambda\lambda 5780, 6284, 4428, 4882$ large-equivalent-width DIBs

Two prominent emission bands appearing in all the low-resolution Copernicus mid-/late-B supergiant spectra and in the high-resolution Copernicus spectrum of  $\beta$  Ori A occur at 1188.3 Å and at 1244.0 Å. In ref. 23, these bands were assigned as Stokes-wave emissions on the transitions C3–6R0 and B10–6R0, respectively. Following the same line of argument employed in Section 4, one can here again account for removal of molecules from the SRS terminal state,  $J'' = 0$  of X6, by a plausible SRS–FWPO scheme (Fig. 20). It will now be shown that, by combining this particular SRS–FWPO scheme with another one to be shortly described, it is possible to make an assignment for what is probably the most famous DIB of all, the one at 5780 Å.

The energy level diagram of Fig. 21 shows a specific H<sub>2</sub> process having high radiative transition probabilities that could be occurring in H<sub>2</sub>-containing clouds around B-type giant and supergiant stars. From (EF4,  $J = 0$ ), a downward parametric oscillation cascade terminating on  $J'' = 0$  of X0 could occur, which would deplete the EF4,  $J = 0$  quantum level. However, such a parametric cascade is not required for the SRS process illustrated in Fig. 21 to occur, since the EF4,  $J = 0$  quantum level could otherwise fluoresce to lower-lying B-state quantum levels in strongly allowed transitions. The X0,  $J'' = 0$  quantum level could thus be repopulated through purely fluorescent channels. For the moment, we assume the existence of the SRS process illustrated in Fig. 21 without further comment about possible optical pathways leading back to  $J'' = 0$  of X0. The existence of a region of absorption near 972.0 Å in Fig. 16 should, however, be noted.

The B''-state quantum level shown at the top left of Fig. 21 is the very same one appearing at the top right of Fig. 20. In the scheme shown in Fig. 20, this quantum level is shown as the resonant intermediate state in a secondary broad-band SRS process driven by Ly- $\beta$  photons trapped in the H<sub>2</sub>-containing cloud by H atoms also present in the cloud. It now becomes apparent that the secondary SRS process shown in Fig. 20 also creates a new SRS–FWPO pathway for the population excited to EF4,  $J = 0$  by the SRS process shown in Fig. 21. *Via* the ‘inverse Raman effect’ (ref. 11), it now becomes possible for visible photons coming from the illuminating star to be absorbed in a band

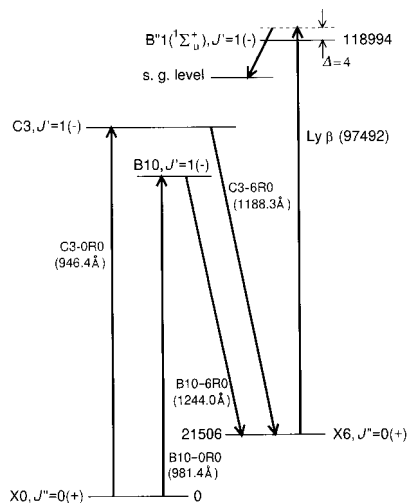


Fig. 20 SRS–FWPO processes explaining some observed strong emission peaks appearing in Copernicus VUV spectra of mid-/late-B supergiants

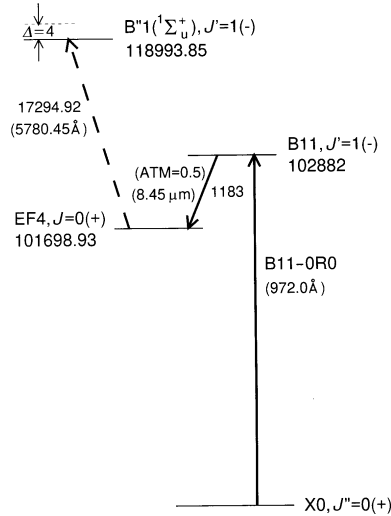


Fig. 21 SRS-FWPO process (when combined with the process shown in Fig. 20) proposed in text as origin of  $\lambda 5780$  DIB

centred at the wavelength of the B''1  $\leftrightarrow$  EF4, R(0) transition, with H<sub>2</sub> molecules that have been excited to EF4,  $J = 0$  now being driven to the (unspecified) singlet-*gerade*-state quantum level shown in Fig. 20. In Fig. 21, we have indicated the exact energies of both the B''1,  $J' = 1$  and EF4,  $J = 0$  quantum levels as listed in ref. 31 and in ref. (6 and 7), respectively. When one converts the difference in energies of these levels,  $17\,294.92\text{ cm}^{-1}$ , to air wavelengths, one obtains  $5780.45\text{ \AA}$ . In Table A1 of his recent review article on the DIBs,<sup>8</sup> Herbig states the rest frame air wavelength of the  $\lambda 5780$  DIB to be  $5780.45 \pm 0.02\text{ \AA}$ . Jenniskens and Désert<sup>4</sup> list the wavelength of this DIB as  $5780.59 \pm 0.05\text{ \AA}$ .

An important point to note concerning the SRS-FWPO mechanisms invoked in the above proposed  $\lambda 5780$  DIB assignment is the following. If the H<sub>2</sub> population that is excited to the unspecified singlet-*gerade*-state quantum level shown at the top right in Fig. 20 makes its way back to  $J'' = 0$  of X0 entirely *via* a downward parametric oscillation cascade, the summed photon momenta of all the light waves comprising either the SRS-FWPO process pictured in Fig. 20, or the one just discussed that combines transitions shown in Fig. 21 and 20, must be conserved, *i.e.*  $\sum \mathbf{k}_i = 0$  where  $\mathbf{k}_i$  is the wavevector of the  $i$ th wave. Hence, all the light waves participating in such SRS-FWPO processes must be coplanar, *i.e.* they must all lie in the 'plane' of the thin H<sub>2</sub>-containing cloud of our model. On the basis of this consideration, an explanation can be offered for the known strong dependence (see, *e.g.* ref. 8) of DIB intensity upon reddening in the line-of-sight. Reddening is generally believed by astronomers to be caused by dust particles of some kind. The presence of dust in the thin H<sub>2</sub>-containing cloud of our model would cause visible photons coming from the illuminating star to be scattered into the plane of the cloud, thereby allowing the photons to participate in SRS-FWPO processes. Without the presence of such dust in the cloud, all visible photons would simply traverse the thin cloud along the line-of-sight, since there are no H<sub>2</sub> or H absorption lines in the visible region of the electromagnetic spectrum to produce elastic scattering at these wavelengths.

In the discussion presented above, it was implied that generation of a broad-band Stokes wave in an SRS process pumped by an intense flux of Ly- $\beta$  photons results in absorption of *ca.*  $5780\text{ \AA}$  photons through the inverse Raman effect. That is, it was

tacitly assumed that the photon flux at *ca.* 5780 Å propagating in the plane of the cloud is not intense enough to produce SRS by itself. On general grounds, one might expect the linewidth of an absorption resulting from the inverse Raman effect to be much narrower than the spectral linewidth of an SRS Stokes wave generated by broad-band pumping, since the former is basically only sensitive to the dispersion in the Raman susceptibility  $\chi^{(3)}$ , whereas the latter depends both on  $\chi^{(3)}$  being large and the linear dispersion being small.<sup>32</sup> With this in view, it is interesting to note that the linewidths of both the  $\lambda 5780$  and  $\lambda 6284$  DIBs are *ca.*  $6 \text{ cm}^{-1}$ , whereas the linewidth of the  $\lambda 4428$  DIB is roughly ten times greater. In the  $\lambda 6284$  DIB assignment to be given below, absorption could again occur *via* a plausible inverse Raman effect process. However, in the case of the  $\lambda 4428$  DIB assignment that will also be offered, absorption *via* the inverse Raman effect is not possible, and one must assume that broad-band light propagating in the plane of the H<sub>2</sub>-containing cloud at wavelengths near 4428 Å is sufficiently intense to reach the SRS threshold. If this speculation should turn out to be correct, the linewidth of a large-equivalent-width DIB should provide an indication of the mechanism through which the DIB is generated, *i.e.* SRS or inverse Raman effect. Of all the DIBs,  $\lambda 4428$  has the largest equivalent width, being almost four times that of  $\lambda 5780$ , for example.

The ATMs calculated in ref. 10, in principle, apply to  $J = 0$  singlet-*gerade*-state quantum levels only. In Fig. 21, the large value indicated (0.5) for the IR transition shown should therefore be reasonably accurate. In ref. 10, ATMs are listed for transitions occurring between EF and B' quantum levels, but not for transitions between EF and B'' quantum levels. However, the potential curve for B'' is similar in shape to that for B', being only vertically displaced from the latter to somewhat higher energies. Therefore, ATMs listed for EF–B' transitions may be used as a guide in obtaining relative ATMs of EF–B'' transitions. The ATM listed for transitions between B'1 and EF3 is very large (2.4), but the ATM listed for transitions between B'1 and EF4 is 60 times smaller (0.04), implying a very small value for the  $17\,295\text{-cm}^{-1}$  transition in Fig. 21. At first glance, this appears to damage seriously the credibility of the  $\lambda 5780$  DIB assignment here being proposed.

The EF4,  $J = 0$  quantum level is also known as the F2,  $J = 0$  quantum level. The wavefunction for this quantum level is primarily localized in the outer ('F') well of the double-welled EF-state potential curve. The wavefunction for the EF3,  $J = 0$  quantum level, also known as the E1,  $J = 0$  quantum level, is primarily localized in the inner ('E') well of the EF-state potential curve. While the energy of F2,  $J = 0$  exceeds that of E1,  $J = 0$  by  $204 \text{ cm}^{-1}$ , the energies of the E1 quantum levels increase with  $J$  faster than the energies of the F2 quantum levels. A cross-over occurs, and at  $J = 3$  the energy of the E1 quantum level exceeds that of F2 by  $80 \text{ cm}^{-1}$ . It is well known that this near degeneracy in energies leads to tunnelling through the barrier existing between the E and F wells. According to *ab initio* calculations presented in ref. 33, the vibrational wave functions of the outer well show a small but significant tunnelling into the inner well and thus into a region that has good Franck–Condon overlap with the vibrational wavefunctions of the B'1 and B''1 states. Experimental verification of tunnelling occurring between E- and F-state quantum levels was reported in ref. 34. The authors of ref. 34 excited various E,F-state quantum levels by two-photon absorption from thermally populated levels of X0. The non-linear absorption was detected by monitoring the subsequent photoionization of the excited E,F quantum levels. The ion signal amplitude for the Q(0) transition to F2 was observed to be 87 times less than that for the Q(0) transition to E1. In each case, the ion signal should vary as the amplitude squared of the rovibronic transition dipole moment between the two-photon-state quantum level and some intermediate-state quantum level. Hence, for the F2,  $J = 0$  quantum level, this transition dipole moment should be about nine times smaller than for the E1,  $J = 0$  quantum level. Thus, one can estimate the ATM value for the  $17\,295\text{-cm}^{-1}$  transition in Fig. 21 to be *ca.* 0.3.

In Fig. 22, an assignment is proposed for the  $\lambda 6284$  DIB that bears some resemblance to the  $\lambda 5780$  assignment just discussed. In this assignment, parahydrogen molecules are again the ‘DIB carriers’. The EF4,  $J = 4$  quantum level can be equally well described as the E1,  $J = 4$  quantum level, that is, its wavefunction is primarily localized in the E well. (The cross-over between E1 and F2 occurs between  $J = 2$  and  $J = 3$ .) Therefore, in obtaining ATMs for transitions between EF4,  $J = 4$  and B-, B<sup>-</sup>, and C-state quantum levels, one uses the values calculated in ref. 10 for transitions involving EF3. Table 1 of ref. 10 indicates very strong coupling between EF3 and C1 (ATM = 3.3), C2 (ATM = 0.2), B<sup>1</sup> (ATM = 2.4), and B<sup>2</sup> (ATM = 1.3), so that a large ATM for EF3  $\leftrightarrow$  D2 can reasonably be assumed. Using the term energy values given in ref. 31 for D2,  $J' = 5(-)$  ( $117\,989.67\text{ cm}^{-1}$ ) and in ref. 6 and 7 for EF4,  $J = 4(+)$  ( $102\,081.05\text{ cm}^{-1}$ ), one obtains  $15\,908.62\text{ cm}^{-1}$  for the difference frequency. This corresponds to an air wavelength of  $6284.17\text{ \AA}$ , well within the limits ( $6284.31 \pm 0.33\text{ \AA}$ ) for the  $\lambda 6284$  DIB given in ref. 4, but somewhat outside the limits ( $6283.86 \pm 0.02\text{ \AA}$ ) given in ref. 8. In ref. 30, results of new measurements of the line positions of some B'  $\leftrightarrow$  X and D  $\leftrightarrow$  X transitions are presented. In Table 7 of ref. 30, the energy for the D2(<sup>1</sup> $\Pi_u^+$ ),  $J' = 5(-)$  quantum level is given as  $117\,990.25\text{ cm}^{-1}$ . This would predict the wavelength of the  $\lambda 6284$  DIB to be  $6283.93\text{ \AA}$ , much closer to the value listed in ref. 8.

In the scheme shown in Fig. 22, no indication is given of how the SRS process that generates a Stokes wave on the C2  $\leftrightarrow$  EF4, P(4) transition is actually pumped. A simple two-photon SRS process would obviously have to start from  $J'' = 2$  of X0. At first glance, it is reasonable to assume that a sizeable steady-state population of parahydrogen molecules might exist in this level, and there is some evidence in the ORFEUS-1 spectra of absorptions occurring from this level, for example, on the transitions B8–0P2 (Fig. 16) and C3–0Q2 (Fig. 19). In Section 4 we also saw that SRS Stokes-wave emission on B16–4P4 resulted from optical pumping of molecules in  $J'' = 2$  of X0. However, no absorption is seen in Fig 19 at the critical wavelength ( $965.8\text{ \AA}$ ) of C2–0R2. One therefore concludes that excitation of the EF4,  $J = 4$  quantum level does not occur *via* a simple SRS process starting from  $J'' = 2$  of X0.

We propose that excitation of the EF4,  $J = 4$  quantum level occurs through the cascaded SRS process diagrammed in Fig. 23. There is abundant evidence in the Coper-

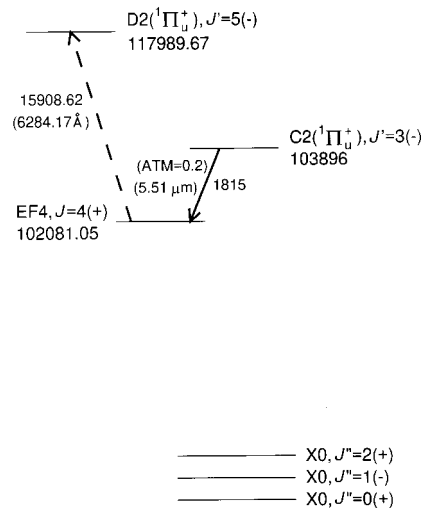


**Fig. 22** SRS–FWPO process (when combined with the process shown in Fig. 23) proposed in text as origin of  $\lambda 6284$  DIB

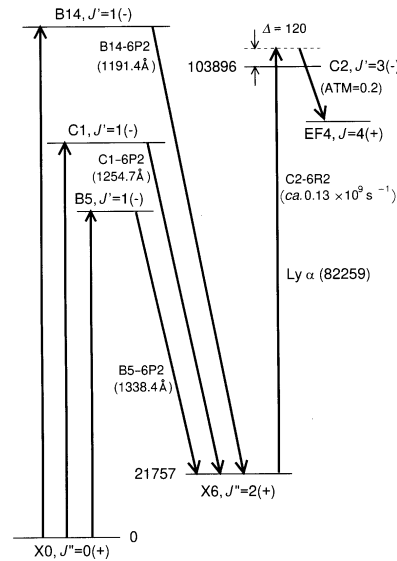


Fig. 23 SRS-FWPO processes proposed in text as mechanisms for excitation of EF4,  $J = 4$  quantum level

nicus and ORFEUS-1 spectra that a specific set of parallel SRS processes is occurring in the H<sub>2</sub>-containing clouds near the stars studied, with each process starting from  $J'' = 0$  of X0 and terminating on  $J'' = 2$  of X6. One finds in the Copernicus spectra emission bands at B2-6P2 (1406.8 Å), B4-6P2 (1359.8 Å), B5-6P2 (1338.4 Å), B8-6P2 (1281.1 Å), B11-6P2 (1232.7 Å), B14-6P2 (1191.4 Å), B15-6P2 (1179.2 Å), B17-6P2 (1156.5 Å), B18-6P2 (1145.9 Å) emission band may also be C0-3Q1), C4-6P2 (1165.2 Å), C2-6P2 (1221.4 Å), C1-6P2 (1254.7 Å), and C0-6P2 (1292.1 Å). The strongest of these transitions are shown in Fig. 23. Regions of absorption corresponding to the R(0)  $Bn \leftrightarrow X0$  and  $Cn \leftrightarrow X0$  pumping transitions are easily identified in the ORFEUS-1 spectra.

One should keep in mind that in broad-band SRS, it is the total pump power at all wavelengths that determines the Stokes-wave gain at any particular wavelength. Thus, for example, the pump power around B5-0R0 contributes to the gain of the Stokes wave around B14-6P2.

The secondary SRS process shown in Fig. 23 could deplete the terminal state ( $J'' = 2$  of X6) of the primary SRS process. One sees in this figure that Ly-α is nearly resonant with the strong ( $0.13 + 9^{-1}$ ) transition C2-6R2. The secondary SRS Stokes wave is assumed to occur on the C2  $\leftrightarrow$  EF4 P(4) transition, as shown in both Fig. 23 and 22. The sequence of two-photon transitions that begins as in Fig. 23, and that then proceeds to some other singlet-*gerade*-state quantum level *via* inverse Raman absorption of *ca.* 6284 Å photons, with  $J' = 5(-)$  of D2 being the resonant intermediate state, is assumed to be part of an overall SRS-FWPO process that returns molecules to  $J'' = 0$  of X0.

In the scheme shown in Fig. 22, absorption of photons near 6284 Å probably occurs *via* inverse Raman absorption. However, unlike the case of the scheme shown in Fig. 20, it is here difficult to isolate an independent SRS process that can generate broad-band coherent radiation centred about the transition between  $J' = 5$  of D2 and a lower-lying singlet-*gerade*-state quantum level. The energies obtained by subtracting Ly-α, Ly-β, Ly-γ, or Ly-δ from the energy of D2,  $J' = 5$  are nowhere close to those of X-state quantum levels, except  $J'' = 4$  of X13. However, D2  $\leftrightarrow$  X13 transitions are extremely weak, relatively speaking. This implies that broad-band coherent radiation centred on the transition from D2,  $J' = 5$  to a lower-lying singlet-*gerade*-state quantum level must

‘come from above’, that is, it must represent a component of a parametric oscillation cascade that originates at some higher-lying level. The existence of such a higher-lying level emerges from our (combined) assignments of the  $\lambda 4428$  and  $\lambda 4882$  DIBs, to be discussed next.

Our assignments for both the  $\lambda 4428$  and  $\lambda 4882$  large-equivalent-width DIBs are shown in Fig. 24. From inspection of this figure, several unusual features are seen to be involved. (1) The uppermost quantum level shown in the figure could be either  $D8(^1\Pi_u^+)$ ,  $J' = 2(+)$  or  $B''6(^1\Sigma_u^+)$ ,  $J' = 2(+)$ . According to ref. 31, both quantum levels have exactly the same energy,  $127\,320.11\text{ cm}^{-1}$ , and both are seen to be optically connected with the two EF-state quantum levels shown, although none of the relevant ATMs were calculated in ref. 10. It is, at this point, impossible to say which of the two equi-energetic upper levels plays the dominant role in the case of each of the two DIBs. (2) In Fig. 24, excitation of the quantum level EF11,  $J = 3$  is shown occurring *via* an SRS process that starts from X0,  $J'' = 3$ . Strong supporting evidence that this process actually occurs can be seen from inspection of Fig. 17. We remarked at the end of Section 4 that no evidence of C4–OR1 absorption exists in this figure. However, the reader should now take note of the intense region of absorption appearing at the C4–OP3 wavelength. In general, absorptions originating from  $J'' = 3$  of X0 appear quite prominently in the ORFEUS-1 spectra, suggesting the existence of a relatively large population in this level, perhaps fed by Stokes-wave emissions. In Section 4, a prominent emission band was assigned to B0–OP3.

From Fig. 19, one sees that strong absorption on either C3–OR1, C3–OR0, or on both of these transitions could be occurring, but it is hard to distinguish among these possibilities, since the frequencies of C3–OR0 and C3–OR1 differ by only  $4\text{ cm}^{-1}$ . In principle, the EF8,  $J = 1$  state could also be populated by an SRS process involving C3–OQ1 as the pumping transition. While there is no strong evidence of absorption occurring at C3–OQ1 in the case of HD 214080, the ORFEUS-1 spectrum of HD 149881 shown in Fig. 25 gives some indication that SRS excited *via* C3–OQ1 may be occurring in the H<sub>2</sub>-containing cloud near this star. (The wavelength scale for the HD 149881 spectrum is less accurate than that for HD 214080.) The non-linear nature of the H<sub>2</sub> absorptions which appear in the ORFEUS-1 spectra of these two B-type halo stars is again illustrated by the fact that the radiative transition probability of C3–OQ1 is 3.5 times that of C3–OR1.

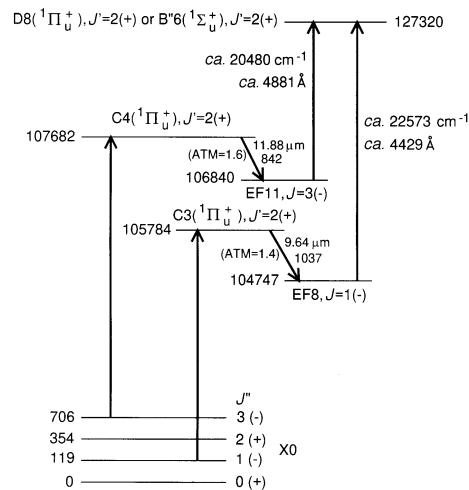
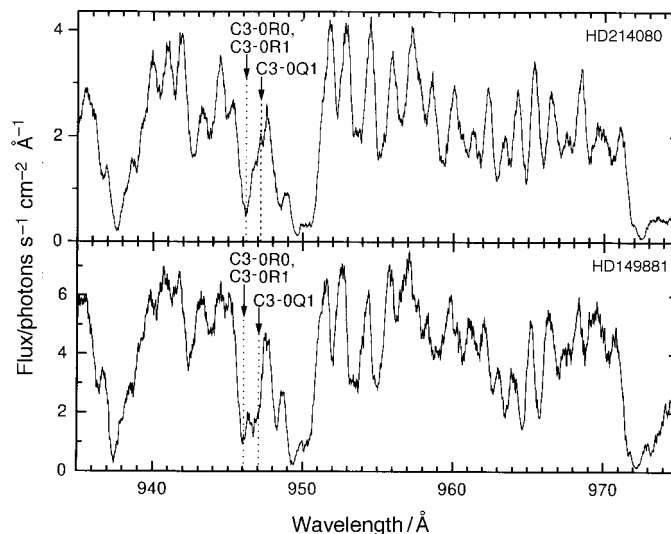


Fig. 24 SRS–FWPO processes proposed in text as origins of  $\lambda 4428$  and  $\lambda 4882$  DIBs



**Fig. 25** Expanded views of ORFEUS-1 spectra of two stars (HD 214080 and HD 149881) that include the wavelength region of the C3–0 transitions discussed in the text.

All the pumping and Stokes-wave transitions shown in Fig. 24 have very large transition dipole moments, making them very favourable for SRS processes. All the quantum level energies have been rounded off in Fig. 24, since the DIBs here are very broad, and the frequencies at their maxima are therefore much less accurately known than in the case of narrower DIBs. The exact frequencies and air wavelengths of the two transitions in Fig. 24 to which the two DIBs are assigned are  $22\,572.78\text{ cm}^{-1}$  ( $4428.89\text{ Å}$ ) and  $20\,480.45\text{ cm}^{-1}$  ( $4881.36\text{ Å}$ ). Ref. 4 lists the wavelengths, linewidths, and equivalent widths (in HD 183143) of the two DIBs as:  $4428.88 \pm 1.35\text{ Å}$ ,  $12.33 \pm 2.06\text{ Å}$ , and  $2488\text{ mÅ}$ ;  $4881.83 \pm 0.65\text{ Å}$ ,  $19.67 \pm 2.38\text{ Å}$ , and  $810\text{ mÅ}$ . In ref. 8, the values of the same quantities are given as:  $4428 \pm 1\text{ Å}$ ,  $18\text{ Å}$ , and  $3400\text{ mÅ}$ ;  $4882\text{ Å}$ ,  $25\text{ Å}$ , and  $890\text{ mÅ}$ . In wavenumber units, the linewidths of these two DIBs given in ref. 4 are  $63 \pm 10\text{ cm}^{-1}$  for the  $\lambda 4428$  DIB and  $82 \pm 10\text{ cm}^{-1}$  for the  $\lambda 4882$  DIB. Within the limits of error, the linewidths could thus possibly be the same.

We hypothesize that enough blue and blue-green light is scattered by dust into the plane of the  $\text{H}_2$ -containing cloud to pump the secondary SRS processes shown in Fig. 24 beyond threshold, thereby opening up new hybrid SRS–FWPO optical pathways. One should here bear in mind that the flux emitted by a  $T = 15\,000\text{ K}$  radiator, when expressed in units of power per unit area per unit frequency interval, peaks somewhere near the blue region of the spectrum. It is also a feature of broad-band SRS that the Stokes-wave gain is remarkably flat, even when the pump radiation spectrally spans a resonance line.<sup>32</sup> The secondary SRS process shown in Fig. 24 is hypothesized to continue in a downward parametric oscillation cascade. If the optical pathway of this downward cascade were to involve, for example, the  $\text{D}2, J' = 5(-)$  quantum level in Fig. 22, this would lead to absorption of photons near  $6284\text{ Å}$  by the inverse Raman effect.

## 6 Conclusions

In trying to account for major deficiencies apparent in the  $\text{H}_2$  DIBs model of ref. 1, we have called attention to what we believe is VUV spectral evidence indicating that there ubiquitously exist thin, cold, tenuous  $\text{H}_2$ -containing clouds located close enough to B-type giant and supergiant stars that the  $\text{H}_2$  molecules in these clouds are driven into a

pattern of coherent oscillations by the VUV blackbody continua emitted by the illuminating stars. At present, we are unable to estimate either the actual distances between the H<sub>2</sub>-containing clouds and the nearby stars or the shapes of the clouds. Our overall conclusion regarding the generation of coherent light in these clouds mostly derives from the following sequence of observations. (1) Emission bands seem to be clearly present in archived (900–1450 Å) spectra of B-type supergiants. (2) These bands appear at exactly the same wavelengths in the spectra of all the mid-/late-B supergiants examined. (3) On the basis of wavelength positions alone, these bands appear to be readily assignable to low- $J''$  H<sub>2</sub> transitions on which one would expect SRS Stokes-wave emission to occur, if viable mechanisms existed to deplete the populations of the terminal states. We then proposed that such mechanisms are provided by the presence of greatly enhanced densities of Ly- $\alpha$ , Ly- $\beta$ , Ly- $\gamma$ , ... *etc.* photons trapped in the H<sub>2</sub>-containing cloud *via* elastic scattering by H atoms, also assumed to be present at high densities in the cloud. It was shown how pumping by the Ly- $\alpha$ , Ly- $\beta$ , Ly- $\gamma$ , ... *etc.* flux can initiate secondary SRS processes which deplete the primary SRS terminal states. It is assumed in our model that the secondary SRS processes then typically initiate downward parametric oscillation cascades which ultimately repopulate the ground state. The overall optical pathways in such schemes can best be described as SRS–FWPO mixing processes in which SRS, inverse Raman absorption, or parametric oscillation can occur at one or more of the  $2n$  ( $n \geq 2$ ) steps. In such SRS–FWPO schemes, conservation of photon momentum holds, *i.e.*

$$\sum_{i=1}^{2n} \mathbf{k}_i = 0$$

This necessitates that all the light waves participating in SRS–FWPO processes be coplanar.

Assignments for several large-equivalent-width DIBs are shown to follow from consideration of specific hybrid SRS–FWPO processes. In order that visible photons emitted by the illuminating star can be absorbed in individual SRS or inverse Raman steps of a hybrid SRS–FWPO process, the photons must be propagating in the ‘plane’ of the thin H<sub>2</sub>-containing cloud. This can only happen if there is also present dust in the cloud to scatter the visible light coming from the star into the plane of the cloud. This provides a simple explanation for the general observation that DIB intensities in given lines-of-sight correlate well with reddening observed in same lines-of-sight.

We are especially grateful to Dr Ralph C. Bohlin for sending us his ASCII-format data files of Copernicus spectra of mid-/late-B supergiant stars. We have benefited from several conversations with Drs Donald S. Bethune and Rodney T. Hodgson and Prof. Stephen E. Harris. P.P.S. and J.H.G. acknowledge the U.S. Army Research Office for having partially supported their work. W.U. acknowledges the Vrije Universiteit and the Research Institute for Condensed Matter and Spectroscopy (COMPAS) for a USF-project grant.

## References

- 1 P. P. Sorokin and J. H. Glowina, *Astrophys. J.*, 1996, **473**, 900.
- 2 T. P. Snow, *Nature (London)*, 1996, **384**, 406.
- 3 R. Loudon, *The Quantum Theory of Light*, Oxford University Press, New York, 2nd edn., 1983.
- 4 P. Jenniskens and F-X. Désert, *Astron. Astrophys. Suppl. Ser.*, 1994, **106**, 39.
- 5 H. Abgrall, E. Roueff, F. Launay, J-Y. Roncin and J-L. Subtil, *J. Mol. Spectrosc.*, 1993, **157**, 512.
- 6 S. Yu and K. Dressler, *J. Chem. Phys.*, 1994, **101**, 7692.
- 7 S. C. Ross and Ch. Jungen, *Phys Rev. A*, 1994, **50**, 4618.
- 8 G. H. Herbig, *Annu. Rev. Astrophys.*, 1995, **33**, 19.
- 9 H. Abgrall, E. Roueff, F. Launay, J-Y. Roncin and J-L. Subtil, *Astron. Astrophys. Suppl. Ser.*, 1993, **101**, 323.

- 10 M. Glass-Maujean, P. Quadrelli and K. Dressler, *At. Data Nucl. Data Tables*, 1984, **30**, 273.
- 11 R. A. McLaren and B. P. Stoicheff, *Appl. Phys. Lett.*, 1970, **16**, 140.
- 12 H. Abgrall, E. Roueff, F. Launay, J-Y. Roncin and J-L. Subtil, *Astron. Astrophys. Suppl. Ser.*, 1993, **101**, 273.
- 13 P. J. Sarre, J. R. Miles, T. H. Kerr, R. E. Hibbins, S. J. Fossey and W. B. Somerville, *Mon. Not. R. Astron. Soc.*, 1995, **277**, L41.
- 14 P. Ehrenfreund and B. H. Foing, *Astron. Astrophys.*, 1996, **307**, L25.
- 15 J. Krelowski and M. Schmidt, *Astrophys. J.*, 1997, **477**, 209.
- 16 B. E. Westerlund and J. Krelowski, *Astron. Astrophys.*, 1988, **203**, 134.
- 17 P. F. Roche, D. K. Aitken and C. H. Smith, *Mon. Not. R. Astron. Soc.*, 1989, **236**, 485.
- 18 W. Ubachs, P. C. Hinnen and E. Reinhold, *Astrophys. J.*, 1997, **476**, L93.
- 19 G. S. Agarwal and W. Harshawardhan, *Phys. Rev. Lett.*, 1996, **77**, 1039.
- 20 S. E. Harris, *Phys. Today*, 1997, **50(7)**, No. 7, 36.
- 21 W. Ubachs and E. Reinhold, 1997, unpublished data.
- 22 R. H. Page, Ph.D. Thesis, University of California, Berkeley, 1987.
- 23 P. P. Sorokin and J. H. Glowina, submitted for publication.
- 24 M. Hurwitz, S. Bowyer, R. Kudritzki and D. J. Lennon, *Astrophys. J.*, 1995, **450**, 149.
- 25 D. C. Morton, *Astrophys. J.*, 1975, **197**, 85.
- 26 N. R. Walborn and R. C. Bohlin, *Pub. Astron. Soc. Pacific*, 1996, **108**, 477.
- 27 J. B. Rogerson and W. L. Upson, *Astrophys. J. Suppl. Ser.*, 1982, **49**, 353.
- 28 J-Y. Roncin and F. Launay, *J. Phys. Chem. Ref. Data (Monograph No. 4)*, 1994, American Physical Society, Woodbury, NY and American Chemical Society, Washington.
- 29 I. Dabrowski, *Can. J. Phys.*, 1984, **62**, 1639.
- 30 H. Abgrall, E. Roueff, F. Launay and J-Y. Roncin, *Can. J. Phys.*, 1994, **72**, 856.
- 31 A. Monfils, *J. Mol. Spectrosc.*, 1965, **15**, 265.
- 32 D. S. Bethune, J. R. Lankard, M. M. T. Loy and P. P. Sorokin, *IBM J. Res. Develop.*, 1979, **23**, 556.
- 33 W. Kolos and L. Wolniewicz, *J. Chem. Phys.*, 1969, **50**, 3228.
- 34 E. E. Marinero, R. Vasudev and R. N. Zare, *J. Chem. Phys.*, 1983, **78**, 692.